JOURNAL OF GEOPHYSICAL RESEARCH, VOL. 106, NO. B2, PAGES 2047–2059, FEBRUARY 10, 2001

Mantle plumes and flood basalts: Enhanced melting from plume ascent and an eclogite component

A. M. Leitch[1], and G. F. Davies

Research School of Earth Sciences, Australian National University, Canberra, ACT

Abstract. New numerical models of starting plumes reproduce the observed volumes and rates of flood basalt eruptions, even for a plume of moderate temperature arriving under thick lithosphere. These models follow the growth of a new plume from a thermal boundary layer and its subsequent rise through the mantle viscosity structure. They show that as a plume head rises into the lower-viscosity upper mantle it narrows, and it is thus able to penetrate rapidly right to the base of lithosphere, where it spreads as a thin layer. This behavior also brings the hottest plume material to the shallowest depths. Both factors enhance melt production compared with previous plume models. The model plumes are also assumed to contain eclogite bodies, inferred from geochemistry to be recycled oceanic crust. Previous numerical models have shown that the presence of nonreacting eclogite bodies may greatly enhance melt production. It has been argued that the eclogite-derived melt would react with surrounding peridotite and refreeze; however, recent experimental studies indicate that eclogite-derived melts may have reached the Earth's surface with only moderate or even minor modification. Combined with an assumed 15 vol % component of eclogite, our models yield a sharp peak in melting of about 1-3 Myr duration and volumes of melt that encompass those observed in flood basalt provinces.

1. Introduction

Flood basalts are vast, geologically brief outpourings of basaltic lava onto the surface of the Earth, and hot spot tracks, which often start at a flood basalt province, are linear trails of much less voluminous volcanism. The "starting plume" or "plume head-plume tail" model has been proposed to explain flood basalts and hot spot tracks [*Morgan*, 1981; *Richards et al.*, 1989; *Campbell and Griffiths,* 1990]. According to this model, a mantle plume begins as an instability in the thermal boundary layer at the core-mantle boundary (CMB) and rises through the mantle as a large, spherical head, with a thinner tail connecting it to the source region. A flood basalt eruption would then result from decompression melting as a hot plume head approaches the surface, while a hot spot track would result as the lithosphere passes over the longer-lived tail.

The starting plume model is based on well-established physics [*Griffiths and Campbell,* 1990] and is consistent with important geophysical and geochemical characteristics of flood basalts and hot spot tracks [*Campbell and Griffiths,* 1990], but it has been criticized because it has seemed that little or no magma would be produced from a plume head unless the lithosphere rifted and allowed the plume material to rise to within less than 100 km of the surface, where substantial pressure-release melting can occur [*White and McKenzie,* 1995]. On the other hand, the rifting model for flood basalts [*White and McKenzie,* 1995] does not seem to be compatible with flood basalts that involve little or no rifting (as in Siberia and the Columbia River basalts) or where a major phase of the eruption preceeds rifting (as in the Deccan Traps) [*Hooper*, 1990]. The plume head model is quite compatible with synrift eruptions, but initial estimates of the amount of prerift magma that would be produced were orders of magnitude less than observed flood basalt volumes.

Two factors that might overcome this discrepancy have been addressed in previous studies. *Farnetani and Richards* [1994, 1995] proposed that plume heads are hotter than had previously been inferred, 350-400°C rather than 100-200°C above ambient mantle. They found that they could obtain large volumes of melt, but the high plume temperature implies surface uplift of 2-4 km, whereas uplifts associated with flood basalts are typically no more than 1 km [*Campbell*, 1998]. Also such high temperatures would produce highly magnesian picrites rather than basalts. Farnetani and Richards attribute the scarcity of picrites to fractional crystallization [*Farnetani et al.*, 1996; *Lassiter et al.*, 1995], but this does not explain why picrites are confined to the early stages of flood basalts [*Campbell*, 1998]. Finally, their models included a relatively soft lower lithosphere which the plumes could displace in order to rise to shallower depths. However, there is little independent evidence that the lithosphere is so readily displaced [*Davies*, 1994].

On the other hand, *Cordery et al.* [1997], following *Campbell et al.* [1995], took note of well-known geochemical evidence that plume composition is different from the source of mid-ocean ridge basalts (MORBs). Trace element and isotopic evidence is commonly interpreted as indicating that plumes have a higher proportion of recycled oceanic crust [*Hofmann and White,* 1982; *Hofmann*, 1997]. This old oceanic crust would exist as eclogite in the upper mantle, and eclogite is expected to melt at substantially lower temperatures than the pyrolite composition of MORB source mantle [*Yasuda et al.*, 1994]. *Cordery et al.* [1997] demonstrated that a hot blob incorporating 15% eclogite would produce volumes of eclogite-derived melt that approached the volumes of flood basalts, even using conventional estimates of plume temperature and with a noneroding lithosphere. However, those models were preliminary, in that the plume head was a pre-

[1]Now at Department of Earth Sciences, Memorial University of Newfoundland, St John's, Canada.

Paper number 2000JB900307.
0148-0227/01/2000JB900307$09.00

scribed blob of uniform temperature, rather than resulting from the ascent of a plume from the CMB.

In this paper we demonstrate, using high-resolution numerical models, that the details of how a plume grows from a thermal boundary layer and rises through the mantle have important effects on the thermal structure of the plume head and on the closeness of the approach of the plume to the Earth's surface. These effects substantially enhance melt production in a plume head. In combination with a 15 vol % eclogitic component, the resulting model plumes readily reproduce observed volumes of flood basalts even with moderate plume temperatures.

We continue our modelling long past the arrival of the plume head to investigate melting in plume tails. We find that the melt rates for the Hawaiian hotspot are best matched with about 3 vol % eclogite in the tail. This apparent difference in the eclogite fraction of heads and tails may be due to nonvertical ascent and entrainment in real tails or to different degrees of eclogite-matrix reaction.

The estimated volumes of eclogite-derived melt provides an upper bound on the amount of magma likely to reach the Earth's surface, since some of the eclogite melt might react with surrounding peridotitic mantle and temporarily refreeze [*Yaxley and Green,* 1998]. However the degree of interaction of eclogitic melts with surrounding mantle is uncertain as it depends on the poorly understood physical processes of melt migration and extraction.

Using new experimental evidence, *Takahashi et al.* [1998] propose that the the main phase of eruption of the Columbia River Basalts may result from partial melting of an eclogitic source with little or no reaction with peridotite. Other flood basalts do show evidence of reaction with peridotite, but their compositions can still be accounted for by assuming an eclogite-derived primary melt. These findings suggest that it is possible for much of the eclogite-derived melt to reach the Earth's surface. Since the main question addressed here is whether the models can approach the observed order of magnitude of flood basalt volumes, we argue that the eclogite melting estimates are a sufficient approximation and that our results support the viability of the plume head model.

2. Background

2.1. Flood Basalts and Hot Spot Tracks

Flood basalts occur roughly every 10 or 20 Myr, both on continents (e.g., Siberian Traps, Columbia River Basalts) and on the ocean floor (e.g., Ontong Java Plateau, Kerguelen Plateau). Volumes are in the range of $0.1 - 10 \times 10^6$ km^3 for continental flood basalts and $10 - 60 \times 10^6$ km^3 for oceanic flood basalts. Dating measurements indicate very rapid emplacement times of 1-3 Myr, giving eruption rates of 0.1-8 km^{3}yr^{-1} on continents and 2-20 km^{3}yr^{-1} on the ocean floor [*Coffin and Eldholm,* 1994]. The present basalt production rate for the entire mid-ocean ridge system is 20 km^{3}yr^{-1}, and for subduction related volcanism it is about 2 km^{3}yr^{-1}. In a global context, melt production from flood basalts is of secondary importance; however, flood basalts have excited much interest both because of their dramatic impact (e.g., they have been linked to mass extinctions [*Richards et al.*, 1989; *Campbell et al.*, 1992]) and because they do not appear to be generated by plate tectonic processes.

Hot spot tracks are linear trails of volcanism which often start at a flood basalt province: for example, the Reunion hot spot track starts at the Deccan Traps, India, and the Tristan hot spot track starts at the Parana flood basalt province, South America. Hot spot tracks are easiest to identify when they occur on oceanic crust, where they manifest as a sequence of volcanic ocean islands (e.g., Hawaii and the Emperor Seamount Chain), but they have also been traced on continents. Hot spots are relatively stationary with respect to one another, and this observation has led to the argument that they must have their origin in the deepest mantle where, because of high viscosity, lateral flow is very slow. The strength of hot spots, as indicated by their buoyancy fluxes, varies a great deal [*Davies*, 1988; *Sleep*, 1990]. For the strongest intraplate hot spot, Hawaii, the volume of volcanic rock above the ocean floor gives a rate of mantle melt production of 0.03 km^{3}yr^{-1} [*Clague and Dalrymple,* 1989]. Subcrustal volcanism probably increases this number by a factor of 2 or 3, but we are left with a melt production rate for strong hotspots which is less than that for flood basalt provinces by 1 or 2 orders of magnitude. Weak hot spots (e.g., Tasmantid [*Duncan and Richards,* 1991]) can be another order of magnitude less productive.

2.2. Eclogite in the Mantle

The geochemical evidence for a larger eclogite component in plume heads (flood basalts) and tails (ocean island basalts) than in the MORB source is discussed by *Cordery et al.* [1997]. This evidence consists of trace element and isotopic data [*Hofmann and White,* 1982], oxygen isotopic data and Re-Os measurements of ocean island basalts, and the FeO content of flood basalts. Together, the evidence suggests that some plumes contain a significant excess component of ancient (~2 Gyr) subducted crust or sediment, although the proportions of eclogite and pyrolite in the source region and the degrees of partial melting of each cannot be determine unambiguously [*Cordery et al.*, 1997].

A current understanding of mantle convection [e.g., *Davies and Richards,* 1992] lends some support to the geochemical evidence. The present subduction rate of oceanic crust into the mantle corresponds to 2% of the entire mantle volume every billion years, so after 4.6 Gyr of Earth history the mantle may well contain 10% or more of eclogite. Since the melting temperature of all mantle minerals increases strongly with pressure [*Boehler*, 1996] and eclogite is probably too cold to melt as it is subducted, it will only be able to melt and react with the surrounding mantle materials when it is returned to the near surface. Throughout its residence in the deep mantle, subducted oceanic crust will be deformed by mantle circulation, but any chemical homogenization (by solid-state reaction) will be minimal.

The distribution of eclogite within the mantle is a matter of debate. Seismic tomography [*van der Hilst et al.*, 1997] indicates that some subducted lithosphere descends very deep in the mantle. It has been suggested that on the basis of differences in rheology and density, the subducted crust might separate from the slab at the 660 km phase transition [*Ringwood*, 1982; *van Keken et al.*, 1996] or at the base of the mantle [*Christensen and Hofmann,* 1994]. According to *Irifune* [1993] and *Kesson et al.* [1994, 1998], the oceanic crust would be about 0.2 g/cm^3 more dense than pyrolite in the upper mantle, 0.2 g/cm^3 less dense between 660 km and about 1100 km, then varying from 0.04 g/cm^3 more dense to possibly 0.03 g/cm^3 less dense at the bottom of the mantle. The uncertainties increase with depth, and as yet, there is no consensus. The relative rheologies of eclogite and pyrolite are even more uncertain.

Mixing efficiency within the mantle is also a matter of debate. Recent numerical studies [e.g., *van Keken and Zhong,* 1999; *van Keken and Ballentine,* 1999] suggest that the mantle should be

evenly mixed; however, this does not accord with geochemical evidence from isotopes of both refractory elements and noble gas isotopes, which point to a more heterogeneous, less depleted, and less degassed reservoir in the lower mantle [*Davies*, 1990; *Hofmann*, 1997; *McDougall and Honda*, 1998]. A combination of factors, including lateral variations in rheology, higher viscosity and minor density stratification, may account for less efficient mixing and longer residence times in the lower mantle [*Davies*, 1990; *Christensen and Hofmann*, 1994]. If these factors inhibit overturning near the CMB, so that there is only slow settling as material is ablated off the bottom of the mantle and channeled into mantle plumes, settling rates are of the order of 150 km every billion years [e.g., *Leitch*, 1995].

There is clear geochemical evidence for differences between the ocean island basalt (OIB) source(s) and the MORB source. In our models we look at the implications for the melting rate if these differences are due to a higher proportion of nonreacting eclogite in the OIB source. This may be due to a difference in the bulk composition of the OIB sources, or it may reflect differences in the scale of heterogeneity and mechanisms of melt extraction (section 6.5). We envisage that eclogite is present in the mantle and in mantle plumes in discrete blobs and stringers which, in the lower mantle in particular, may have dimensions up to kilometer size.

2.3. Previous Work

Farnetani and Richards [1994] modeled a plume head as an isolated isothermal sphere of pyrolite composition released at 2000 km depth and allowed to rise and flatten against the lithosphere. The lower mantle had a viscosity of about 10^{22} Pa s, the upper mantle was 1 or 2 orders of magnitude less viscous, and the lithosphere was up to the same viscosity as the lower mantle. For initial temperature anomalies ΔT between 300 and 400°C and lithosphere thicknesses of 50 and 110 km, they obtained melt rates comparable with flood basalts. Melting occurred in a single pulse of about 10 Myr duration in a thin disc along the top of the flattened plume head. The lower lithosphere in most of their models was, however, very weak [cf. *Davies*, 1994], and this allowed the plume to rise to relatively shallow depths. For a stiffer lithosphere they found melt volumes were reduced by a factor of 2 to 3.

Cordery et al. [1997] carried out the first numerical simulations of the melting of eclogite in plume heads, with models similar to those of *Farnetani and Richards* [1994], except that the mantle was always topped by lithosphere a thousand times more viscous than the upper mantle. In general agreement with *Farnetani and Richards* [1994], they found that for pyrolite plumes with ΔT of 100-300°C, very little melt formed. A "squeeze" layer of normal mantle was trapped between the plume head and the base of the lithosphere, limiting how high the plume head could rise, and the lithosphere was not thinned at all by reheating or plume-related shear. For the hottest plume heads (ΔT = 300°C) and the thinnest lithosphere (50 km) of their runs only 0.15×10^6 km^3 of melt was produced. However, when the plume head had 15 wt % eclogite mingled into it the models yielded up to 5×10^6 km^3 of melt within 3 Myr. The maximum degree of melting experienced by the eclogite was between 10 and 35%, and again melting occurred in a thin disc at the top of the flattened plume head.

Farnetani and Richards [1995] looked at melting and entrainment in pyrolite starting plumes, again with a relatively weak lithosphere. For temperature contrasts across the CMB ΔT_{CMB} of 400°C, they found about 20% partial melting occurred in a flattened oval with a radius of about 400 km at the top of the plume axis, between depths of about 80 and 180 km. They found there was very little melting of entrained mantle material: more than 90% of melting material originated from within 100 km of the CMB.

3. Numerical Models

3.1. Equations and Boundary Conditions

We ran the simulations using the finite difference, multigrid program CONMG, which has been successfully compared with published benchmarks [*Blankenbach et al.*, 1989] and unpublished finite element solutions [*Davies*, 1995]. CONMG solved the equations for infinite Prandtl number, incompressible flow with Newtonian rheology, and the heat equation including the effects of latent heat. In axisymmetric cylindrical coordinates the momentum equations in dimensionless units are

$$0 = -\frac{\partial p'}{\partial r'} + \frac{\partial \sigma'_{rr}}{\partial r'} + \frac{\partial \sigma'_{rz}}{\partial z'} + \frac{\sigma'_{rr} - \sigma'_{\phi\phi}}{r'} \tag{1a}$$

$$0 = -\frac{\partial p'}{\partial z'} + \frac{\partial \sigma'_{zz}}{\partial z'} + \frac{\partial \sigma'_{rz}}{\partial r'} + \frac{\sigma'_{rz}}{r'} - T', \tag{1b}$$

where the components σ_{ij} of the deviatoric stress tensor are

$$\sigma'_{rr} = \eta' \frac{\partial u'_r}{\partial r'}, \qquad \sigma'_{\phi\phi} = \eta' \frac{u'_r}{r'},$$
$$\sigma'_{zz} = \eta' \frac{\partial u'_z}{\partial z'}, \qquad \sigma'_{rz} = \tfrac{1}{2}\eta' \left(\frac{\partial u'_r}{\partial z'} + \frac{\partial u'_z}{\partial r'}\right). \tag{1c}$$

Vertical distance z is measured downward. The dimensionless heat equation can be written

$$\frac{DT'}{Dt'} = \frac{1}{Ra}\left[\frac{1}{r'}\frac{\partial}{\partial r'}\left(\frac{\partial T'}{\partial r'}\right) + \frac{\partial^2 T'}{\partial z'^2}\right] - L'\frac{DX}{Dt'}. \tag{2}$$

where D/Dt' is the material derivative, L' is the latent heat, and X is the depletion fraction. Symbols are defined in the Table 1.

The domain was a cylinder with radius 1500 km and depth 3000 km, with the plume rising up the axis. A uniform 256x512 grid provided a very high resolution of 6 km. Boundary conditions were free-slip and reflecting on the sides, no-slip constant temperature (0°C) at the top and free-slip constant temperature (T_{CMB}) on the bottom. The background mantle had a constant potential temperature T_p of 1300°C. The temperature anomaly at the core-mantle boundary ΔT_{CMB} was set between 200 and 520°C in different simulations in order to yield reasonable temperature anomalies ΔT_m for plumes in the melting zone of the upper mantle.

The temperature in the top boundary layer had an error function profile

$$T(z) = T_m \operatorname{erf}(z/h), \tag{3}$$

where h is the "lithosphere thickness." For oceanic lithosphere the relationship between thickness and age is

$$h = 2\sqrt{\kappa t}; \tag{4}$$

h was reset to a desired thickness (60 or 90 km, corresponding to

Table 1. Notation and Values Used in Simulations

Parameter	Definitions	Values/Units
	Dimensionless Variables	
E^*	activation energy	$E/[R(T_p+273)]$
L'	latent heat	$\Delta S_m (T+273)/c_p T_p$
p'	dynamic pressure	$p\,d^2/(Ra\eta_0\kappa)$
Nu	Nusselt number	$Q\,d/(k\,A\,\Delta T_0)$
Ra	Rayleigh number	$\rho\,g\,\alpha\Delta T_0\,d^3/\eta_0\kappa$
T'	temperature	T/T_p
T^*	absolute temperature ratio	$(T+273)/(T_p+273)$
t'	time	$t\,Ra\,\kappa/d^2$
u_i'	velocity component ($i = r, z$)	$u_i\,d/(Ra\,\kappa)$
X	depletion fraction	
r'	radial distance	r/d
z'	depth	z/d
η'	dynamic viscosity	η/η_0
θ	temperature fraction	$(T-T_S)/(T_L-T_S)$
	Dimensional Variables	
A	horizontal surface area	m^2
c_p	specific heat	$1000\ J\,kg^{-1}\,K^{-1}$
d	depth of the mantle	3×10^6 m
E	diffusion creep activation energy	$3\times10^5\ J\,mol^{-1}$
g	acceleration of gravity	$9.8\ m\,s^{-2}$
h	lithosphere thickness	60, 90 km
k	thermal conductivity	$4\ W\,m^{-1}\,°C^{-1}$
Q	heat flux	W
R	universal gas constant	$8.317\ J\,K^{-1}mol^{-1}$
t_1	time from start of simulation	s, Myr
t_2	time from start of melting	Myr
T_p	background potential temperature	1300°C
z_0	reference depth	3.3×10^5 m
ΔS_m	entropy of melting	$400\ J\,kg^{-1}\,K^{-1}$
ΔT_0	reference temperature difference	T_p or $2\Delta T_{CMB}$
ΔT_{CMB}	CMB temperature jump	200 – 520°C
α	thermal expansivity	$2\times10^{-5}\ K^{-1}$
η_0	reference viscosity	5×10^{19} Pa s
κ	thermal diffusivity	$10^{-6}\ m^2\,s^{-1}$
ρ	reference density	$4000\ kg\,m^{-3}$
	Subscripts	
0	reference value	
CMB	core mantle boundary	
m	melting	
H	Hawaiian plume	
L	liquidus	
S	solidus	

oceanic lithosphere ages of 28.5 and 64 Myr) as the plume head approached.

Initially, the bottom boundary had an error function profile where the layer thickness h_{CMB} varied linearly, usually from 150 km at the axis to 113 km at the far edge. This variation ensured that flow along the bottom was inwards toward the axis and that off-axis ring boundary instabilities were avoided.

Viscosity was both temperature- and depth-dependent. It had the form

$$\eta(T,z) = \eta_0 \exp[E^*(1/T^* - 1)]\,H(z,B)\exp[(lnG)(z-z_0)], \quad (5)$$

where η_0 is the reference viscosity. $H(z,B)$ is a blurred step function equal to 1 in the upper mantle and B in the lower mantle. Therefore there was a step increase by a factor of B at 660 km depth superimposed on a continuous increase with depth by a factor of G. We used $B = 20$ and $G = 10$. An increase in viscosity with depth of about 2 orders of magnitude is predicted by post-glacial rebound [*Forte and Mitrovica,* 1996] and the relative motion of hot spots [*Steinberger and O'Connell,* 1998], and a factor of about 20 increase through the transition zone is indicated by independent evidence from subduction zone geoids [*Hager*, 1984]. The viscosity was capped at $2000\eta_0$. The effect of mineral phase transitions on density, latent heat, and thermal expansivity was neglected. The Rayleigh number Ra (Table 1) was 5.5×10^8.

3.2. Melting of Pyrolite and Eclogite

We assumed a plume composition of either pyrolite or 15 vol % eclogite. This eclogite fraction (15 vol %) was chosen as a reasonable estimate of the quantity of eclogite within the mantle (section 2.2) and also to facilitate comparison with work by *Cordery et al.* [1997], whose choice of 15 wt % (14.4 vol %) was based on how much excess eclogite component the plume could carry.

The implementation of melting in the code is explained by *Leitch et al.* [1998]. Basically, melting began when material crossed the solidus (Figure 1). Melting absorbed latent heat and produced a volume of partial melt, both at rates proportional to the melt rate, DX/Dt:

$$\frac{DX}{Dt} = \frac{dX}{d\theta}\frac{D\theta}{Dt}. \quad (6)$$

X is the depletion fraction, that is, the melt fraction of the melting component (either pyrolite or eclogite), and θ is the normalized temperature within the liquidus-solidus interval (Table 1). For eclogite, in the absence of firm data, we assumed for simplicity that X varied linearly from 0 to 1 between solidus and liquidus

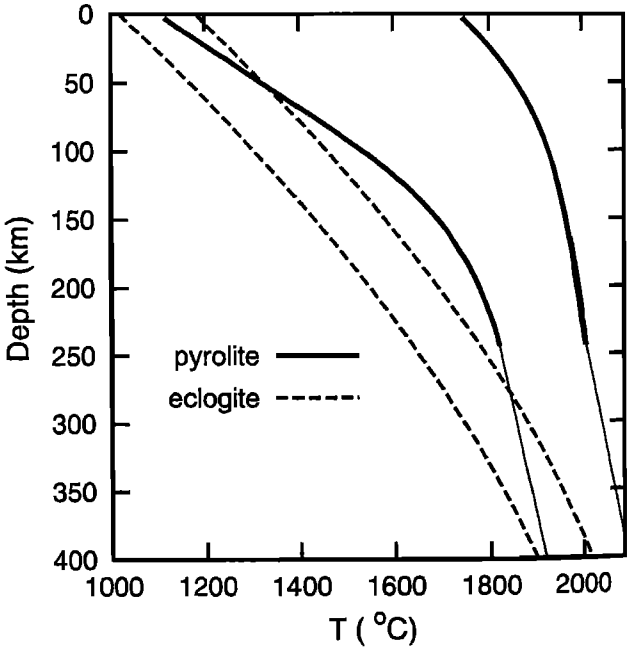

Figure 1. Liquidus and solidus curves used in the melting simulations. Curves for pyrolite from *McKenzie and Bickle* [1988] (thick solid lines), extrapolated assuming a constant liquidus-solidus interval (thin solid lines). Curves for eclogite from *Yasuda et al.* [1994] (dashed lines). Depth scale assumes mantle is topped by 7 km of oceanic crust. The influence of the adiabat was removed in the simulations.

(i.e., $dX/d\theta$ was constant). For pyrolite we used the empirical relationship [*McKenzie and Bickle*, 1988]

$$\frac{dX}{d\theta} = 2.068 - 8.113\,\theta + 8.964\,\theta^2. \quad (7)$$

We assumed that there was no reaction between eclogite melt and the surrounding mantle matrix. The issue of melt-matrix reaction is discussed in section 6.1. Because kilometer-scale eclogite blobs would rapidly thermally equilibrate with their surroundings [*Cordery et al.*, 1997], the mantle material was treated as a continuum where the latent heat was that of eclogite multiplied by the volume fraction of eclogite. The total integrated melt was presumed to appear instantly on the surface. We neglect advection of heat due to percolation of the melt and variations in melt volume due to reaction or freezing. In terms of melt volumes produced, these terms are of secondary importance, and moreover, they depend on the method of melt extraction (e.g., through porous flow or a network of fissures), and this has not been firmly established. Therefore we restrict ourselves to a simple representation of melting and do not claim an accuracy on absolute melt volume of better than about 50%.

The upward motion of the plume heads was driven solely by the buoyancy forces resulting from the temperature anomaly of the plume. For simplicity, although these are not negligible, buoyancy forces due to the presence of eclogite, depleted residue, or the presence of melt were ignored. In the upper mantle at least, eclogite is denser than pyrolite. A crude estimate of the temperature excess δT in the plume relative to the surrounding mantle necessary to counteract this negative buoyancy is

$$\delta T = \frac{\Delta f_e (\rho_e - \rho_0)}{\alpha\,\rho_0}. \quad (8)$$

If we assume the surrounding upper mantle contains 10% eclogite, then for an excess eclogite component Δf_e of 0.05, given ρ_e = 3500 kg/m^3 and ρ_0 = 3330 kg/m^3, δT is 85°C. If there is no excess eclogite, only a difference in the scale of heterogeneity, then there is no compositional buoyancy. Sinking rates of kilometer-scale eclogite blobs within the plume are negligibly slow.

In eclogite-bearing plumes melting of pyrolite was not considered: melt rates of pyrolite were always orders of magnitudes less than those for eclogite. Time was measured from the beginning of the simulations (t_1) and from the start of melting (t_2).

4. Plume Heads and Flood Basalts

A summary of results is given in Table 2 and discussed in section 4.2. We first describe the rise and melting of the plume head over a time period of tens of millions of years (section 4.1). In sections 4.3 and 4.4 we focus on the melting in the first few million years after the start of melting for plume compositions of pyrolite and 15 vol % eclogite.

4.1. Rising Plume

Figure 2 is a time sequence showing a plume head rising through the mantle and impinging on the bottom of the lithosphere. Figure 2f shows the background viscosity structure defined in (5). A plume head forms from an instability in the bottom boundary layer and rises up the cylinder axis (Figure 2a). The plume head is elongated in the vertical (Figure 2b) because the background viscosity decreases with height. At the viscosity step the plume head necks down (Figure 2c), and the central, hottest part of the plume rises quickly through the lower viscosity upper mantle and impinges on the bottom of the lithosphere (Figure 2d), trapping very little normal mantle above it. The outer part of the plume head follows through more slowly (Figure 2e) and spreads out in a thin, flat layer.

The risetime through the upper mantle is very quick, and the plume head spreads out over a timescale of about 5 Myr. In Fig-

Table 2. Summary of Results[a]

Run Conditions			Results for Heads							Results for Tails			
Run	ΔT_{CMB}	h	t_{1m}	t_{2max}	ΔT_m	z_m	z_{ave}	mr_{max}	V_2	ΔT_m	z_m	z_{ave}	mr/mr_H
Pyrolite													
BB[b]	520	60	34.15	0.12	450	570-390	470	1.0	0.65	370	190-80	140	2.7
BE[b]		90	34.16	0.12	450	570-390	470	1.0	0.30		190-105	150	1.3
GG	400	60	57.5	1.2	335	160-110	135	0.06	0.085	305	140-80	120	1.0
GF		90	58.0	0.8	345	165-145	155	0.0008	0.0007		140-105	125	0.24
IB	300	60	96.1	2.7	250	100-125	110	0.006	0.008	235	115-80	100	0.13
15% *Eclogite*													
BH	520	60	34.15	0.35	445	400-80	260	18	20	370	365-60	240	8
BG		90	34.16	0.4	445	510-170	300	11.5	13		365-80	250	6
GH	400	60	57.25	0.45	345	340-80	225	5.9	7.6	305	295-115	205	5.5
GI		90	57.26	0.5	345	340-170	245	2.7	4.0		295-130	215	4
IA	300	60	95.0	0.5	260	270-90	190	2.3	2.9	235	260-105	185	<4.6
I		90	95.12	1-2	255	260-150	200	0.6	1.0		245-115	185	2.3
J	200	60	179.0	0.8	175	210-90	165	0.83	0.8	115	200-105	160	1.0
JA		90	179.15	1	175	210-150	180	0.17	0.28				

[a] h is lithosphere thickness (km); t_{1m} is time after beginning of run at which melting starts; t_{2max} is time of maximum melt rate, measured from t_{1m} for 15% eclogite and h of 60 km; z_m is melting depth range at t_{max} (km); ΔT_m is temperature anomaly at which melting starts; z_{ave} is average melting depth at t_{max} (km); mr_{max} is maximum melt rate (km^{3}yr^{-1}); V_2 is melt volume in first 2 Myr (10^6 km^3); mr/mr_H is ratio of tail melt rate to that of Hawaiian plume (about 0.1 km^{3}yr^{-1}).

[b] Melting rates and depths for plume heads are not quantitatively reliable (see text, section 4.2).

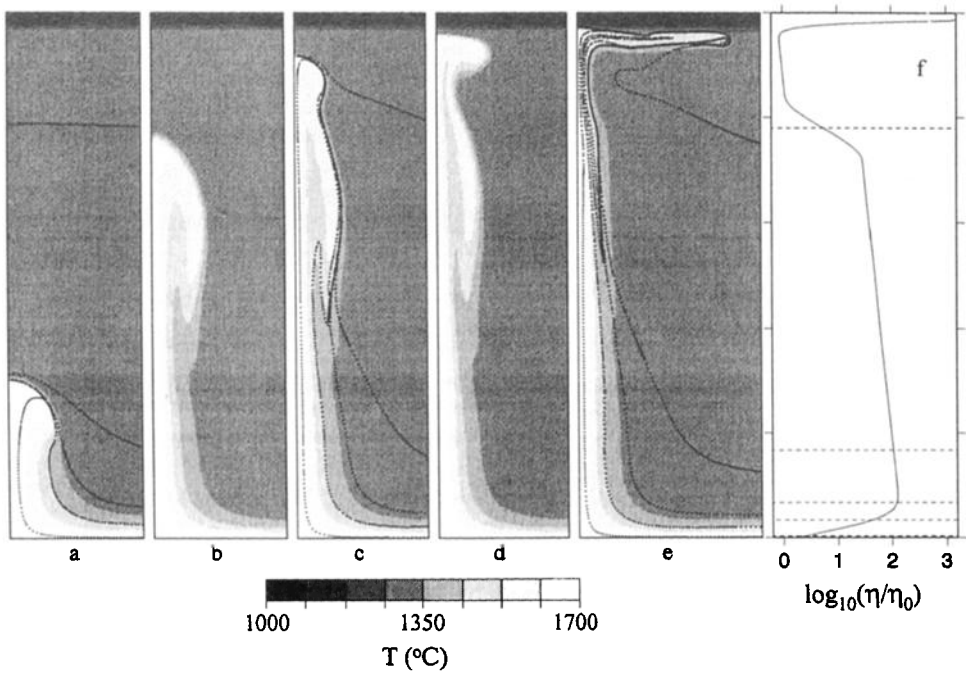

Figure 2. Time sequence showing the temperature field of a plume head rising through the mantle, assuming the depth- and temperature-dependent rheology given in equation (5). Case GG. Times t_1 after start of simulation are (a) 45.8 Myr; (b) 56.8 Myr; (c) 57.4 Myr; (d) 57.7 Myr; (e) 62.8 Myr. Melting starts at t_1 = 57.5 Myr. Contour interval is 70°C. Only part of the domain closest to the axis is shown. Alternate frames show tracer particles, originally in horizontal lines at 10, 100, 200, and 500 km from the CMB and 660 km from the surface. (f) Background viscosity structure and the original positions of the lines of tracer particles.

ure 2e, the outer part of the plume head is still feeding through into the upper mantle but only very slowly: at this point the dynamics is similar to that of the quasi-steady plume tail. The actual times for the rise and spreading of the plume head depend on the buoyancy of the head and the viscosity of the mantle, but the same qualitative behavior was observed in all models.

Figure 3 shows the melting behavior for a plume similar to that in Figure 2 but with a lower initial buoyancy (see Figure 3 caption) over a period of 65 Myr, for plume compositions of pyrolite (dashed line) and 15% eclogite, starting from when eclogite begins to melt.

The curves both rise from zero to an initial peak within about half a million years. This peak, which produces high melt rates for about 3 Myr, coincides with the arrival of the central part of the plume head, which has quickly risen through the upper mantle (Figure 2d). A second, broader peak, which in the case of the pyrolite plume is actually higher than the first, is associated with the slow draining, over about 15 Myr, of the outer part of the plume head into the upper mantle (Figure 2e). At still longer time, melting is due to quasi-steady state upflow of the plume tail.

Plume heads arise from a boundary layer instability at the CMB, and their initial buoyancy may be quite variable because the boundary layer may vary in thickness and composition due to unsteady flow in the deep mantle, which is affected by the irregular subduction of oceanic plates. A plume tail arises from the draining of the boundary layer into an existing conduit: its buoyancy flux is determined by its "catchment area" and the core heat flux, which may vary from place to place. Thus the buoyancy of a plume head is not necessarily related to the buoyancy flux in its tail, and so when looking at the melt rate produced specifically by plume heads, we restrict ourselves to the melting peak observed in the first 4.5 Myr.

4.2. Comparison of Models

The results for plume head melting are given in the left side of Table 2. For both pyrolite and eclogite compositions, the peak melt rate mr_{max}, and the total melt volume V_2 produced in the first 2 Myr after the start of melting decrease sharply as the plume temperature ΔT_{CMB} decreases or the lithosphere thickness h increases. Because the solidus curve for pyrolite is steeper than

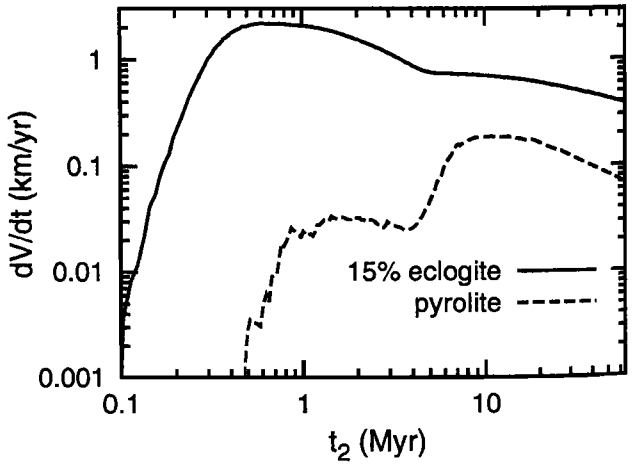

Figure 3. Melt rate versus time. Plume compositions of pyrolite (dashed line) and 15 vol % eclogite. Time t_2 counted from the start of melting of the eclogite-bearing plume. Cases similar to GG and GH (ΔT_{CMB} = 400°C, h = 60 km), except with thinner initial bottom boundary layer thickness (80 km on axis to 60 km on far edge) and lower resolution of 128x256 cells (12 km).

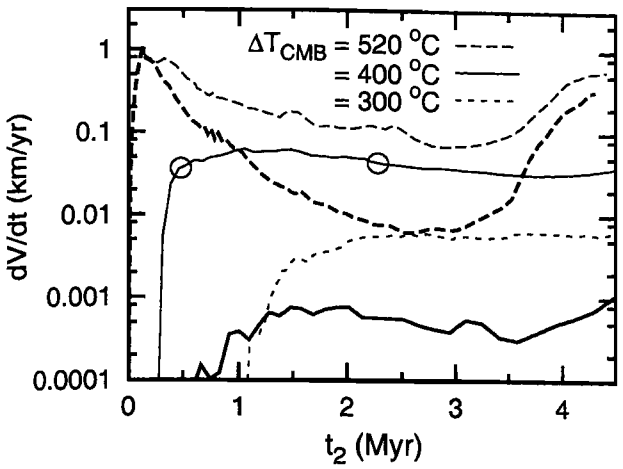

Figure 4. Melt rate versus time for plumes with pyrolite composition. For each value of ΔT_{CMB}, time counted from the start of melting of eclogite-bearing plumes with h = 60 km. Thin lines indicate h = 60 km, and thick lines indicate h = 90 km. Circles indicate times of snapshots in Figure 5.

that for eclogite (Figure 1), melt rates change more rapidly with h for pyrolite plumes.

As the head rises and melts, the depth range of melting z_m and the axial temperature anomaly when the rising material starts to melt ΔT_m vary greatly with time: the values in Table 2 apply at the time of peak melt rate t_{max}. Eclogite-bearing plumes usually start to melt deeper than pyrolite plumes. For the hottest plumes, pyrolite melts deeper because the liquidus-solidus curves cross at depth (Figure 1): However, these curves were determined for depths less than 250 km [*McKenzie and Bickle,* 1988] and so the results are not quantitatively reliable. For pyrolite, t_{max} occurs before the plume encounters the lithosphere (see z_m in Table 2) because the solidus has a shallow slope at depth and plume head is very hot when it first rises into the upper mantle and cools quickly with time. Eclogite may become exhausted along the plume axis. The shallow melting for eclogite with h = 60 km occurs in the outer part of the plume stem.

Melting rates and volumes for plumes of pyrolite composition only approach those of flood basalt provinces for case BB with ΔT_m = 450°C and h = 60 km. Hot eclogite-bearing plumes, particularly under thin lithosphere (BH, BG, GH) generate melt rates appropriate to oceanic plateaus, and only the coolest plume and the thickest lithosphere (JA) produce low melt rates.

4.3. Pyrolite Plumes

Figure 4 shows the total melt rate versus time for plumes of pyrolite composition. Except for the hottest case where the plume head intersects the solidus at depth (see above), the melt rate is relatively flat, and it is very sensitive to both plume temperature and lithospheric thickness, decreasing by roughly an order of magnitude for each 100°C decrease in plume temperature, or as the lithosphere thickness increases from 60 to 90 km.

A clue to the low magnitude and relatively uniform melt rate with time can be found by examining the melt rate field in the plume head. Figure 5 shows temperature and melt rate fields for plume head GG at the two times indicated by the circles on Figure 4. The region in which melting occurs is very small, along the axis at the top of the plume, and there is little difference in the position or magnitude of melting in the 3 Myr interval. Only the hottest part of the plume actually melts, and material in this regions originates from very close to the CMB [*Farnetani and Richards,* 1995]. The tracer particles that outline the melting region in Figure 5 originate from 10 km above the CMB. Melting in these plume heads is virtually indistinguishable from the

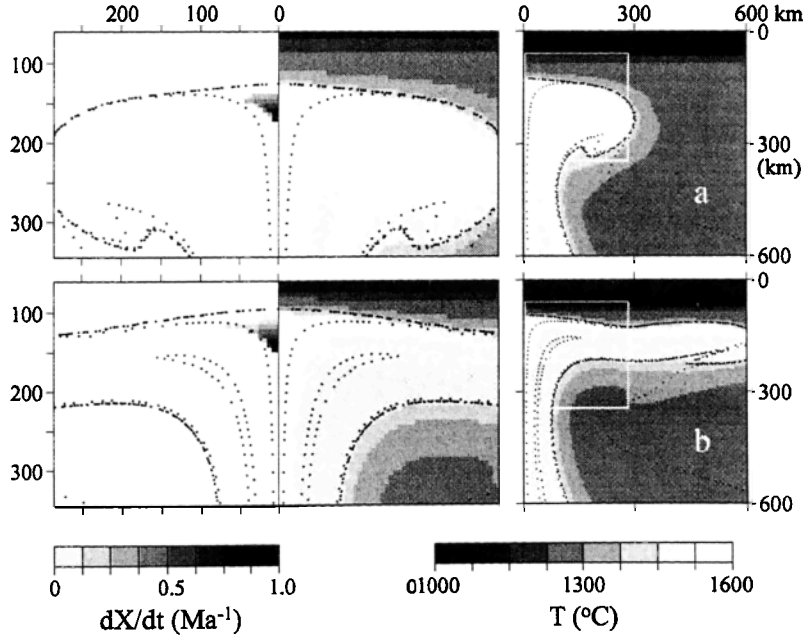

Figure 5. Temperature and melt rate fields for plume heads with pyrolite composition. Case GG, ΔT_{CMB} = 400°C, h = 60 km. (right) Temperature in 600 km x 600 km region at top of axis. (left) Closeups of melt rate and temperature in a region of depth and radius 285 km, indicated by the white squares on the right. Scales on frames show horizontal and vertical distances in km from the top of the axis of the domain. Tracer particles as in Figure 2. (a) t_1 = 57.7 Myr, t_2 = 0.5 Myr; (b) t_1 = 59.5, t_2 = 2.3.

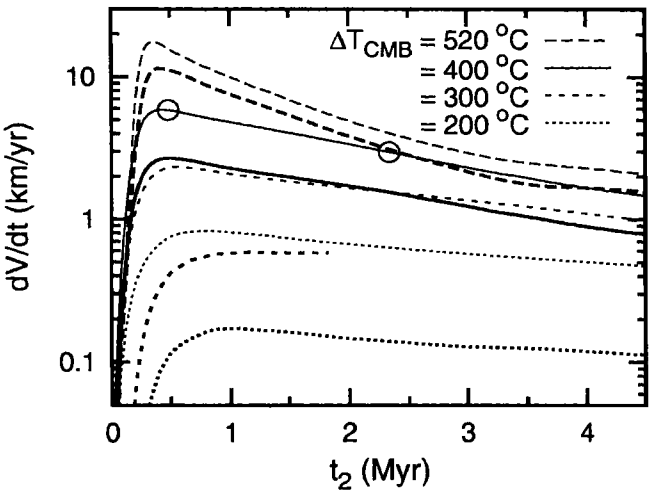

Figure 6. Melt rate versus time for plumes with 15 vol % eclogite component. For each ΔT_{CMB}, time t_2 counted from the start of melting of plume with h = 60 km. Thin lines indicate h = 60 km, and thick lines indicate h = 90 km. Circles indicate times of snapshots in Figure 7.

longer term "plume tail" melting, except that as tail flow becomes established there is a faster flux up the axis and hence the melt rate actually increases with time.

4.4. Eclogite-Bearing Plumes

Figure 6 shows curves of melt rate as a function of time for plumes containing 15 vol % eclogite. As for a pyrolite plume, the melt rate is highly dependent on both h and ΔT_{CMB}. Most important, melt production rates comparable with flood basalts (0.5-18 km^3yr^{-1}) are achieved over reasonable timescales (1-3 Myr).

Figure 7 shows a close up of the plume head as it approaches the lithosphere. The frames are at similar time intervals t_2 after the start of melting as those in Figure 5. There are striking differences between the melt fields in Figures 7 and 5. Eclogite melts over a much deeper and wider region. The melt rates dX/dt in Figure 7 are an order of magnitude higher than those in Figure 5, but dX/dt in Figure 7 is for the eclogite component only (15% of the mantle). The melt rates of the *total* mantle material (dX_p/dt and $f_e dX_e/dt$) are comparable. The most significant differences are in the spatial extent of melting. Eclogite melts at much greater depths than pyrolite (about 130 km deeper, see Table 2), and along the plume axis it finishes melting, because the eclogite component has been exhausted, at about the same time as the pyrolite starts to melt. This can be understood from examining Figure 1: the liquidus for the eclogite lies below the solidus for the pyrolite. (Note that the latent heat of melting of the eclogite reduces the temperature in the plume.) While a pyrolite plume only melts at the top of the plume axis, the melting region for a plume with an eclogite component is much wider, although the highest melt rates are still restricted to the axis of the plume.

Figure 7a also shows that there is a minor degree of melting in the mantle just above the plume head as the head heats the mantle just above it and erodes the bottom of the lithosphere a little so that the eclogite component in the mantle at its "normal" potential temperature (1300°C) just starts to melt due to decompression.

Figure 6 shows that as ΔT_{CMB} (and ΔT_m) increases, the melting peak is more pronounced because at higher plume temperatures more of the plume head outside the plume axis is hot enough to melt at sublithosphere depths.

5. Plume Tail Melting and Hawaiian Hot Spot

Hot spots are thought to arise from a long-term, quasi-steady draining of the boundary layer at the CMB. To look at plume tail melting, we continued our simulations for longer time at lower resolution (256x128 elements, for a cell size of about 12 km). Results are summarized and compared with results for Hawaii in Tables 2 and 3. For Hawaii, we assume that the total heat flux $Q_H = 2\times10^{11}$ W, the melt rate mr_H = 0.1 km^3yr^{-1} [*Davies*, 1988], and the lithosphere thickness h_H = 105 km [*Clague and*

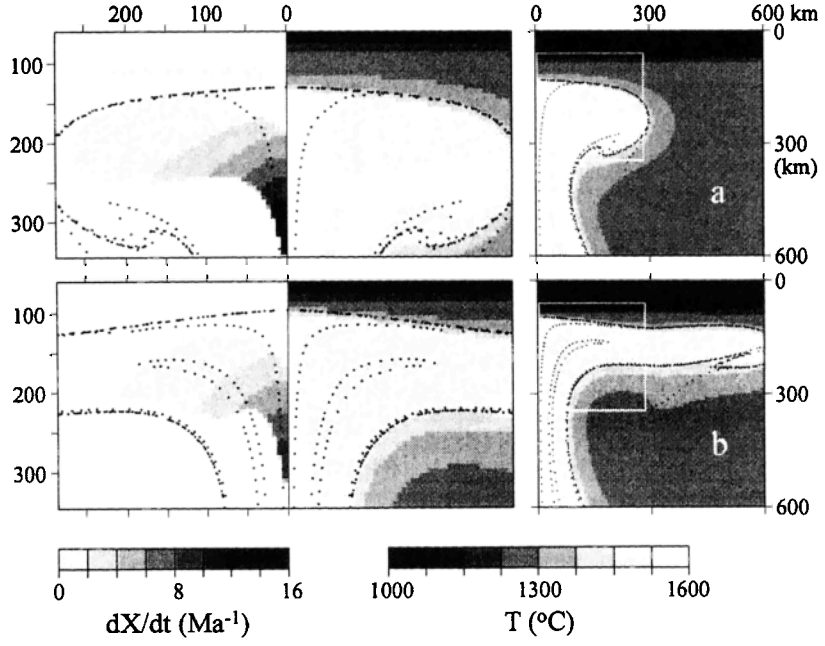

Figure 7. Greyscale plots of temperature and melt rate in plume heads with 15 vol % eclogite component. Case GH, ΔT_{CMB} = 400°C, h = 60 km. See caption for Figure 5. (a) t_1 = 57.7 Myr, t_2 = 0.5 Myr; (b) t_1 = 59.6, t_2 = 2.3.

Table 3. Conditions for Tail Melting Runs[a]

ΔT_{CMB}	t_m	t_2	Q_{CMB}/Q_H	Q_{UM}/Q_H
520	34	20	1.1	1.3
400	57	26	0.7	1.0
300	95	35	0.5	0.7
200	179	52	0.3	0.4

[a] t_m is time after start when plume head starts to melt (Myr); t_2 is time after t_m when tail melting is measured (Myr); Q_{CMB}/Q_H is ratio of total basal flux to 2×10^{11} W (flux for Hawaiian plume); Q_{UM} is flux into upper mantle at time $t_m + t_2$.

Dalrymple, 1989]. The asymptotic steady state in our simulations is not particularly realistic (it involves ring subduction of the lithosphere) so we measured the melt rate at time t_2 when the plume head had spread out to the edges of the computational domain. Since the plume head spreads at a rate roughly proportional to its buoyancy, t_2 is inversely proportional to ΔT_{CMB}.

In a steady state the flux of heat Q_{UM} up the plume tail is the same as the flux of heat Q_{CMB} into the source boundary layer from the core. At high Rayleigh numbers the steady state heat flux from a horizontal boundary is, from dimensional arguments,

$$Nu = c\, Ra^{1/3}, \tag{9}$$

where the Nusselt number Nu is the normalized heat flux (Table 1), and the constant c is about 0.1 [*Turner*, 1979]. We calculated Q_{CMB} by integrating the conductive flux ($k\, dT/dz$) over the bottom boundary and by integrating the advected heat ($\rho c_p v (T - T_p)$) over the plume tail as it passes into the upper mantle. In our simulations, Q_{CMB} approaches a steady value soon after the plume head reaches the bottom of the lithosphere. Using appropriate values $\Delta T_0 = 2\Delta T_{CMB}$ and $\eta_0 = 10^{21}$ Pa s in the definitions of Nu and Ra (see Table 1), we obtain $c = 0.079 \pm 0.002$. Q_{CMB} varies from 0.3 to 1.1 times the flux of the Hawaiian plume and so within reasonable values for the Earth. There is a time lag between the flux across the CMB and the flux in the upper part of the mantle, so the tail heat flux Q_{UM} at the time we measured the melt rate is somewhat higher than the base flux Q_{CMB} (Table 3). The temperatures ΔT_m are comparable with estimates of hot spot temperatures. These temperatures are significantly lower than the CMB temperatures and also lower than the plume head temperatures (Table 2). Figure 8 shows a plot of the centerline temperature of a plume tail, which decreases steadily, due to horizontal diffusion, as it rises through the lower mantle, then drops more abruptly as the tail passes into the upper mantle and thins.

Table 2 lists the melt rates and the depth range of melting for pyrolite and 15% eclogite plume compositions. Melt rate varies about an order of magnitude on either side of the Hawaiian melt rate, with eclogite-bearing plumes having consistently higher values. The closest match to the Hawaiian plume for heat flux and lithosphere thickness is with cases GF and GI. GF has a melt rate only 20% of the Hawaiian melt rate, whereas GI has a melt rate a factor of 4 greater.

Seeking a closer match, we ran two further simulations with a lithosphere thickness of 105 km to match that underneath Hawaii. We used plume compositions of pyrolite (GK) and 3 vol % eclogite (GN) (Table 4). For the pyrolite composition, the melt rate was lower than Hawaiian melt rates even if we assume no subcrustal melting. For 3% eclogite it was comparable. Figure 9

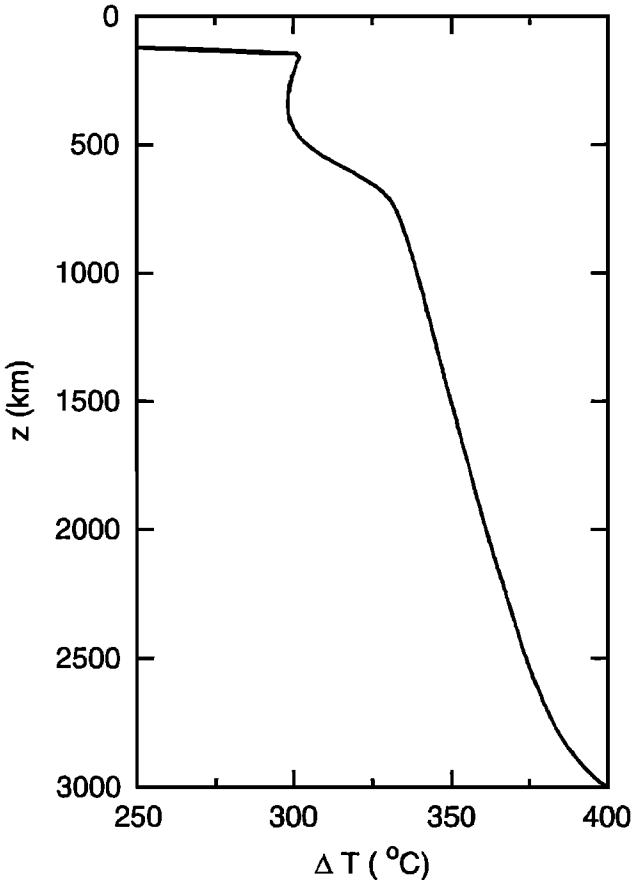

Figure 8. Centerline temperature profile for plume tail, case GK.

shows temperature and melt rate fields for plume tail melting. Eclogite melts much deeper than pyrolite, and finishes melting (because the eclogite is exhausted) before the pyrolite starts to melt. In both cases, melting is concentrated in the center of the plume tail, though it does extend radially at the top. Melting occurs at the top of the plume where the flow is diverging and upward flow is slowing. The average vertical flow rate is about 850 km Myr^{-1} (85 cm yr^{-1}) in the eclogite melt range and 120 km Myr^{-1} (12 cm yr^{-1}) in the pyrolite melt range.

The "catchment area" of our model plumes is 7×10^6 km^2, which is about 5% of the surface area of the CMB. *Sleep* [1990] estimates that the Hawaiian hot spot contributes about a tenth of the total flux from 40 hot spots. Assuming heat flux is proportional to catchment area, the catchment area in the models is reasonable.

In summary, we were able to produce a reasonable match to many of the features of the Hawaiian hot spot, including the buoyancy flux, temperature, lithosphere thickness, and CMB catchment area. To match the melt rate as well requires a few percent of eclogite in the plume.

Table 4. Extra Tail Melting Runs[a]

Run	Composition	ΔT_{CMB}	h	z_m	z_{ave}	mr/mr_H
GK	pyrolite	400	105	140-106	130	0.12
GN	3% eclogite	400	105	305-150	225	1.0

[a] ΔT_{CMB}, h, z_m, z_{ave}, mr/mr_H; see Table 2.

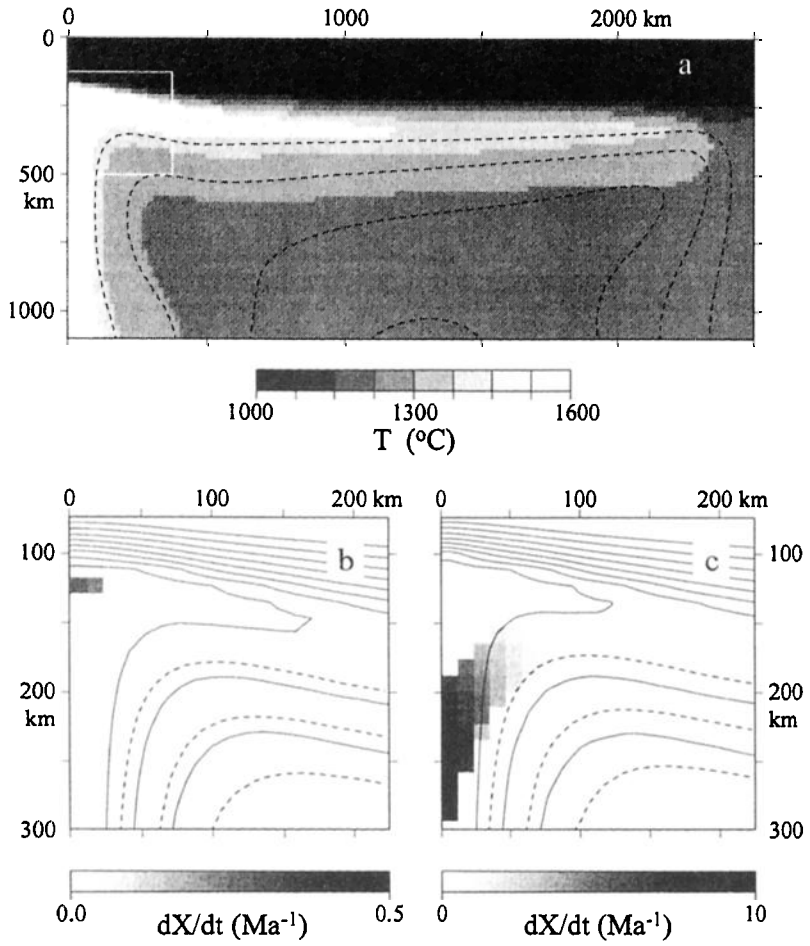

Figure 9. Plume tail melting. (a) Temperature field (greyscale) and streamlines in the upper mantle for case GK (ΔT_{CMB} = 400°C, h = 105 km). Contour interval for streamlines 4×10^{-8} (dimensionless units). White square indicates the area shown in Figures 9b and 9c. (b) Melt rate (greyscale), contours of temperature (fine lines) and streamlines (bold dashed lines) for case GK (pyrolite). Streamline contour interval 2×10^{-8}, half that in Figure 9a. (c) As for Figure 9b for case GN (3 vol % eclogite). Distances marked on frames are measured from top of domain axis.

6. Discussion

6.1. Reaction of Eclogite with Surrounding Peridotite

There is no question that primary eclogite-derived melt would be out of equilibrium with peridotite. However, the degree of reaction and the ultimate amount and composition of the melt depends on how much of the original melt comes into contact with peridotite and on the conditions under which melting occurs.

Yaxley and Green [1998] found that at 3.5 GPa (110 km depth) eclogite-derived melts are very siliceous (dacitic) at low melt fractions, and these react with pyrolite to form a more "fertile" peridotite. At temperatures at or below the pyrolite solidus, this fertile peridotite produces a volume of low-silica (nepheline-normative) picritic melt comparable with the original volume of eclogite. Picritic mantle melts may pond and fractionate near the base of the crust [*Lassiter et al.*, 1995; *Farnetani et al.*, 1996], but nepheline normative picrites would fractionate to produce low-silica basalts. *Yaxley and Green* [1998] argued that flood basalts are more siliceous than this.

On the other hand, *Takahashi et al.* [1998] found experimentally that melting a basaltic composition at 2 GPa (70 km depth) by 30-50% (at a temperature of 1300-1350°C) yields a basaltic andesite that matches the main major and trace element features of the main eruptive phase of the Columbia River Basalts (CRB). Thus the CRBs can be explained by partial melting of the eclogite component of a plume source at low temperatures and pressures, with minimal reaction with peridotite. Other flood basalts are more typically less siliceous (olivine tholeiites), and *Takahashi et al.* [1998] argue that these flood basalts can be accounted for by eclogite melting at higher temperatures and pressures, with some reaction with peridotite. *Kogiso et al.* [1998] show that melting a homogeneous mixture of basalt and peridotite yields low-silica alkali basalts that are typical of many OIBs. Thus it is argued that the full range of OIBs and flood basalts can be explained by melting of heterogeneous plume heads and tails containing eclogitic bodies in a peridotite matrix.

The explanation of the full range of flood basalt compositions is likely to involve some additional processes. Others have argued that ponding and fractionation (mentioned above) and crustal contamination, which has been inferred on the basis of orthopyroxene abundance and other chemical signatures [*Irvine*, 1970; *Campbell*, 1985], would account for the higher silica content of many continental flood basalts.

These petrological questions remain to be fully resolved, but the results of *Takahashi et al.* [1998] indicate that it is plausible that eclogite-derived melts are only moderately modified by reac-

tion with peridotite during their ascent to the surface. We conclude that our use of eclogite-derived melt volumes, though approximate, is adequate for deciding whether a plume model can reproduce the observed order of magnitude of flood basalts.

6.2. Melt Sources and Entrainment for Plume Heads

For a starting plume, in contrast to a uniform temperature blob, the highest temperatures and therefore the most favourable position for melting occur along the plume axis. The models of *Farnetani and Richards* [1995] showed that for a pyrolite starting plume, all melting material originates from a source region within 100 km of the CMB. Our high-resolution simulations show that the source region may be even more restricted. The tracer particles surrounding the pyrolite melting region in Figure 5 originated from within 10 km of the CMB. For eclogite melting (Figure 7) most material originated from within 10 km of the CMB and almost all from within 100 km.

Upon passing through a significant step in viscosity between the lower and upper mantle, the outer part of the plume head is folded, as can be seen from the folding of the lines of tracers in Figures 2e, 5, and 7, so that material from different depths in the mantle is mingled on a medium scale. If most melting occurs as the plume head first approaches the lithosphere, then these models indicate that flood basalts arise from the central part of the plume, which has its source very close to the CMB as described above. However, if melting of the plume head occurs some time after emplacement as a result of rifting [e.g., *Leitch et al.*, 1998], then the melting material may have its source from a range of depths in the mantle. These models have not yet spanned the full range of plausible plume temperatures and head sizes, so more extensive melting of plume heads remains a possibility.

6.3. Melting Column

For pyrolite compositions, melting occured only at the top of the plume axis (Figure 5), whereas an eclogite component may start to melt at nearly 300 km depth and have completely melted some distance below the lithosphere (Figure 7). Since pyrolite starts to melt roughly when eclogite has melted completely (Figure 1), the melting column may be 200 km in extent.

The long, narrow melting column of an eclogite-bearing plume would have an important implication if the melt became sufficiently interconnected and concentrated that viscous resistance from adjacent solid matrix is small. Such an interconnected melting column of height H exerts an overpressure $\Delta P = \Delta\rho g H$ at the top of the column. For $\Delta\rho$ = 300 kg/m^3 this gives $\Delta P/H = 3\times10^3$ Pa/m or 30 bar/km. *Kelemen et al.* [1997] suggest that dike generation beneath mid-ocean ridges might occur for overpressures of about 500 bars. Once this pressure is exceeded, dikes would form and quickly drain the melt.

An interconnected melting column of 150 km would generate an overpressure of 0.45 GPa (4.5 kbar). Although there is considerable uncertainty about the strength of the lithosphere, it certainly could not sustain such an enormous overpressure, and we would expect the lithosphere at the top of such a melting column to rupture as the plume head first approached. This process may account for the narrow, cylindrical low seismic velocity features seen in the lithosphere under the Deccan [*Kennett and Widiyantoro,* 1999] and the Parana [*VanDecar et al.*, 1995] flood basalt provinces. These features have been interpreted to be warm and/or compositionally distinct remnants of the plume responsible for the flood basalts. (In the case of the Parana, the thermal signature would have dissipated since plume arrival in the Jurassic.) The diameter of the cylindrical features (about 200 km) corresponds well with both the central region of the plume in our models (where most intense melting takes place (see Figure 7)) and recent seismic observations of the plume tail under Iceland [*Allen et al.*, 1999].

This concentration of melting near the central part of the plume is also in agreement with observations from giant radiating dike swarms, which are associated with flood basalts [*Ernst and Buchan,* 1997]. Flow patterns in the dikes show magma upflow through the crust in a central area with a radius of a few hundred kilometers and then lateral transport of magma for distances of more than a thousand kilometers [*Ernst and Baragar,* 1992].

6.4. Melt Volumes From Plume Heads and Tails

In this study we looked at melting of plume heads and tails under the lithosphere. We found that for a pyrolite composition melting rates were very low unless the plume temperature was very high and the lithosphere thin (Table 2). Moreover, for a pyrolite composition, there was very little difference between the melt rate associated with the arrival of the plume head and that associated with the longer-term plume tail melting. This was because only the hottest plume material, situated along the axis of the plume, was able to melt. The large, warm plume head spread without melting.

For a plume containing 15 vol % eclogite, in contrast, there was a large peak in the melt rate as the plume head arrived at shallow depth because the outer part of the plume head was warm enough for the eclogite component to melt (Figure 7). The melt rates of a few million cubic kilometers per million years, and the peak width of a few million years (Table 2), match observations of flood basalt provinces.

The melt rates of plume tails containing 15 vol % eclogite were a few times less than the peak melt rates but still higher than observed in hot spot tracks. The observed melt rate of the Hawaiian plume was matched by a plume tail containing 3 vol % eclogite. It is conceivable but unlikely that plume tails actually contain a lower proportion of eclogite than plume heads, since they arise from the same region of the mantle. On the other hand, the circumstances in which magma ascends and erupts are substantially different for heads than for tails. The degree of reaction with surrounding mantle might well be systematically different, as we discuss in section 6.5. In addition, our axisymmetric plume tails are vertical, but real plume tails will be tilted from the vertical by the plate-scale flow in the mantle, and this will cause some thermal entrainment into the tail [*Richards and Griffiths,* 1988, 1989; *Griffiths and Richards,* 1989]. The tail temperature would thus be cooler and the melting substantially reduced by this effect.

6.5. Differences Between Heads, Tails and MORBs

When considering eclogite-periodite reaction there are two "end-member" extremes. In one extreme, fine-scale stringers of eclogite might partially melt and the melts propogate slowly by porous flow, maximizing contact and reaction with the matrix. If the neighboring matrix was residual harzburgite from the slab, reaction may even generate a pyrolite composition. In another extreme, large bodies of eclogitic melt might propagate rapidly upward through existing dike pathways [*Maaloe*, 1998] with little alteration.

While both extremes are unlikely, we might expect the MORB source to be closest to the first scenario, plume heads closest to the second, and plume tails to be in between. This might help explain the different quantities of nonreacting eclogite that our

numerical models require to match observed melt rates in MORB (~0%), plume tails (~3%), and plume heads (~15%) without the need for the total eclogite fraction to be different. We argued in section 6.4 that real plume tails may be cooler than our axisymmetric models. Lower overall melting rates may also lead to a significant difference in the upward propogration of the melt.

Provided that eclogite in plumes is not mixed on a fine scale, the higher melting rates (of eclogite) in plume heads might lead to more rapid propagation of the melt, to greater propagation through dikes, and thus to less reaction with peridotite, particularly if the eclogite stringers are aligned with the plume axis by flow and particularly if the melt can punch through the lithosphere in one location (section 6.3).

There are three factors which would tend to mute the effect of eclogite in the source of MORBs relative to plumes [*Hofmann*, 1997]. First, the MORB source, the upper part of the upper mantle, is arguably more intimately mixed than the CMB, where plumes originate [*Davies*, 1990] (although the scale of mixing in plumes near the surface has yet to be determined). Second, the results of *Yaxley and Green* [1998] suggest that eclogite would start to melt and react at asthenospheric depths before material entered the main melt zone under a ridge. Third, there is a high degree of partial melting of pyrolite at a mid-ocean ridges (~13%), which would dilute the effect of eclogite heterogeneities.

7. Conclusions

Our numerical models show that the location, timing, and degree of melting in mantle plume heads is sensitive to the viscosity structure of the mantle through which the plume ascends and the thickness and strength of the lithosphere. When our models include a significant eclogite component, they yield the same order of magnitude as the observed eruption volumes in flood basalt provinces. While our calculation of eclogite melt volume is an end-member, recent experimental results indicate that eclogite-derived melt may not be greatly modified during ascent and eruption. In any case our main conclusion survives even if the erupted volume is substantially less than the volume of melt generated in the eclogitic source regions.

Acknowledgments. The code was run on the Fujitsu VAP Supercomputer at the Australian National University's Supercomputer Centre. A.M.L. is grateful for support from the NSERC grants of M. Rochester and G. Quinlan, which enabled the completion of this work. The paper benefited from thoughtful reviews from D. Bercovici, C. Farnetani, and P. van Keken.

References

Allen, R.M., et al., The thin hot plume beneath Iceland, *Geophys. J. Int., 137,* 51-63, 1999.

Blankenbach, B., et al., A benchmark comparison for mantle convection codes, *Geophys. J. Int., 98,* 23-38, 1989.

Boehler, R., Melting of mantle and core materials at very high pressures, *Philos. Trans. R. Soc. London, Ser. A, 354,* 1265-1278, 1996.

Campbell, I.H., The difference between oceanic and continental tholeiites: A fluid dynamic explanation, *Contrib. Mineral. Petrol., 91,* 37-43, 1985.

Campbell, I.H., The mantle's chemical structure: Insights from the melting products of mantle plumes, in *The Earth's Mantle: Composition, Structure and Evolution,* edited by I.N.S. Jackson, pp. 259-310, Cambridge Univ. Press, New York, 1998.

Campbell, I.H., and R.W. Griffiths, Implications of mantle plume structure for the evolution of flood basalts, *Earth Planet. Sci. Lett., 99,* 79-93, 1990.

Campbell, I.H., G.K. Czemansky, V.A. Fedorenko, R.I. Hill, and V. Stepanov, Synchronism of the Siberian Traps and the Permian-Triassic boundary, *Science, 258,* 1760-1763, 1992.

Campbell, I.H., M.J. Cordery, and G.F. Davies, The relationship between mantle plumes and continental flood basalts, in *Proceedings of the International Field Conference and Symposium on Petrology and Metallogeny of Volcanic and Intrusive Rocks of the Midcontinent Rift System,* pp. 23-24, Contin. Educ. and Ext., Univ. of Minn., Duluth, 1995.

Christensen, U.R., and A.W. Hofmann, Segregation of subducted oceanic crust in the convecting mantle, *J. Geophys. Res., 99,* 19,867-19,884, 1994.

Clague, D.A., and G.B. Dalrymple, Tectonics, geochronology and origin of the Hawaiian-Emperor volcanic chain, in *The Geology of North America,* vol. N, *The Eastern Pacific Ocean and Hawaii,* edited by E.L. Winterer, D.M. Hussong, and R.W. Decker, pp. 188-217, Geol. Soc. of Am., Boulder, Colo., 1989.

Coffin, M.F., and O. Eldholm, Large igneous provinces: crustal structure, dimensions, and external consequences, *Rev. Geophys., 32,* 1-36, 1994.

Cordery, M.C., G.F. Davies, and I.H. Campbell, Genesis of flood basalts from eclogite-bearing mantle plumes, *J. Geophys Res, 102,* 20,179-20,198, 1997.

Davies, G.F., Ocean bathymetry and mantle convection, 1, Large-scale flow and hotspots, *J. Geophys. Res., 93,* 10,467-10,480, 1988.

Davies, G.F., Mantle plumes, mantle stirring and hot-spot chemistry, *Earth Planet. Sci. Lett., 99,* 96-109, 1990.

Davies, G.F., Thermomechanical erosion of the lithosphere by mantle plumes, *J. Geophys. Res., 99,* 15,709-15,722, 1994.

Davies, G.F., Penetration of plates and plumes through the mantle transition zone, *Earth Planet. Sci. Lett., 133,* 507-516, 1995.

Davies G.F., and M.A. Richards, Mantle convection, *J. Geol., 100,* 151-206, 1992.

Duncan, R.A., and M.A. Richards, Hotspots, mantle plumes, flood basalts, and true polar wander, *Rev. Geophys., 29,* 31-50, 1991.

Ernst, R.E., and W.R.A. Baragar, Evidence from magnetic fabric for the flow pattern of magma in the Mackenzie giant radiating dyke swarm, *Nature, 356,* 511-513, 1992.

Ernst, R.E., and K.L. Buchan, Giant radiating dyke swarms: Their use in identifying pre-Mesozoic Large Igneous Provinces and mantle plumes, in *Large Igneous Provinces: Continental, Oceanic and Planetary Flood Volcanism, Geophys. Monogr. Ser.,* vol. 100, edited by J.J. Mahoney and M.E. Coffin, pp. 297-333, AGU, Washington, D.C., 1997.

Farnetani, C.G., and M.A. Richards, Numerical investigations of the mantle plume initiation model for flood basalt events, *J. Geophys. Res., 99,* 13,818-13,833, 1994.

Farnetani, C.G., and M.A. Richards, Thermal entrainment and melting in mantle plumes, *Earth Planet. Sci. Lett., 136,* 251-267, 1995.

Farnetani, C.G., M.A. Richards, and M.S. Ghiorso, Petrological models of magma evolution and deep crustal structure beneath hotspots and flood basalt provinces, *Earth Planet. Sci. Lett., 143,* 81-94, 1996.

Forte, A.M., and J.X. Mitrovica, New inferences of mantle viscosity from joint inversion of long-wavelength mantle convection and post-glacial rebound data, *Geophys. Res. Lett., 23,* 1147-1150, 1996.

Green, D.H., and T.J. Falloon, Pyrolite: A Ringwood concept and its current expression, in *The Earth's Mantle: Composition, Structure and Evolution,* edited by I.N.S. Jackson, pp. 311-378, Cambridge Univ. Press, New York, 1998.

Griffiths, R.W., and I.H. Campbell, Stirring and structure in mantle starting plumes, *Earth Planet. Sci. Lett., 99,* 66-78 1990.

Griffiths, R.W., and M.A. Richards, The adjustment of mantle plumes to changes in plate motion, *Geophys. Res. Lett., 16,* 437-440, 1989.

Hager, B.H., Subducted slabs and the geoid: constraints on mantle rheology and flow, *J. Geophys. Res., 89,* 6003-6015, 1984.

Hofmann, A.W., Mantle geochemistry: The message from oceanic volcanism, *Nature, 385,* 219-229, 1997.

Hofmann, A.W., and W.M. White, Mantle plumes from ancient oceanic crust, *Earth Planet. Sci. Lett., 57,* 421-436, 1982.

Hooper, P.R., The timing of crustal extension and the eruption of continental flood basalt formation, *Nature, 345,* 246-249, 1990.

Irifune, T., Phase transformations in the Earth's mantle and subducting slabs: Implications for their compositions, seismic velocity and density structures and dynamics, *Island Arc,* 2, 55-71, 1993.

Irvine, T.N., Origin of chromitite layers in the Muskox intrusion and other stratiform intrusions: A new interpretation, *Geology, 5,* 597-611, 1970.

Kelemen, P.B., G. Hirth, N. Shimizu, N. Spiegelman, and H.J.B. Dick, A review of melt migration processes in the adiabatically upwelling mantle beneath oceanic spreading ridges, *Philos. Trans. R. Soc., London, Ser. A, 355,* 1-35, 1997.

Kennett, B.L.N., and S. Widiyantoro, A low seismic wavespeed anomaly beneath northwestern India: a seismic signature of the Deccan plume?, *Earth Planet. Sci. Lett., 165,* 145-155, 1999.

Kesson, S.E., J.D. FitzGerald, and J.M. Shelley, Mineral chemistry and density of subducted basaltic crust at lower mantle pressures, *Nature, 327,* 767-769, 1994.

Kesson, S.E., J.D. FitzGerald, and J.M. Shelley, Mineralogy and dynamics of a pyrolite lower mantle, *Nature, 393,* 252-255, 1998.

Kogiso, T., K. Hirose, and E. Takahashi, Melting experiments on homogeneous mixtures of peridotite and basalt: Application to the genesis of ocean island basalts, *Earth Planet. Sci. Lett., 162,* 45-61, 1998.

Lassiter, J.C., D.J. DePaolo, and J.J. Mahoney, Geochemistry of the Wrangellia flood basalt province: Implications for the role of continental and oceanic lithosphere in flood basalt genesis, *J. Petrol., 36,* 983-1009, 1995.

Leitch, A.M., Effects of temperature and mantle dynamics on estimates of the thermal conductivity in the deep mantle, *Phys. Earth Planet. Inter., 89,* 89-108, 1995.

Leitch, A.M., G.F. Davies, and M. Wells, A plume head melting under a rifting margin, *Earth Planet. Sci. Lett., 161,* 161-177, 1998.

Maaloe, S., Extraction of primary abyssal thoeliite from a stratified plume, *J. Geol., 106,* 163-179, 1998.

McDougall, I., and M. Honda, Primordial solar noble-gas component in the Earth: Consequences for the origin and evolution of the earth and its atmosphere, in *The Earth's Mantle, Composition, Structure and Evolution,* edited by I.N.S. Jackson, pp. 159-187, Cambridge Univ. Press, New York, 1998.

McKenzie, D.P., and M.J. Bickle, The volume and composition of melt generated by extension of the lithosphere, *J. Petrol., 29,* 625-679, 1988.

Morgan, W.J., Hotspot tracks and the opening of the Atlantic and Indian Oceans, in *The Sea,* vol. 7, edited by C. Emiliani, pp. 443-487, Wiley-Interscience, New York, 1981.

Richards, M.A., and R.W. Griffiths, Deflection of plumes by mantle shear flow: Experimental results and a simple theory, *Geophys. J., 94,* 367-376, 1988.

Richards, M.A., and R.W. Griffiths, Thermal entrainment by deflected mantle plumes, *Nature, 342,* 900-902, 1989.

Richards, M.A., R.A. Duncan, and V.E. Courtillot, Flood basalts and hotspot tracks: Plume heads and tails, *Science, 246,* 103-107, 1989.

Ringwood, A.E., Phase transformations and differentiation in subducted lithosphere: Implications for mantle dynamics, basalt petrogenesis, and crustal evolution, *J. Geol., 90,* 611-43, 1982.

Sleep, N.H., Hotspots and mantle plumes: Some phenomenology, *J. Geophys. Res., 95,* 6715-6736, 1990.

Steinberger, B., and R.J. O'Connell, Advection of plumes in mantle flow: Implications for hotspot motion, mantle viscosity and plume distribution, *Geophys. J. Int., 132,* 412-434, 1998.

Takahashi, E., K. Nakajima, and T.L. Wright, Origin of the Columbia River basalts: Melting model of a heterogeneous plume head, *Earth Planet. Sci. Lett., 162,* 63-80, 1998.

Turner, J.S., *Buoyancy Effects in Fluids,* Cambridge Univ. Press, New York, 1979.

VanDecar, J.C., D.E. James, and M. Assumpcao, Seismic evidence for a fossil mantle plume beneath South America and implications for plate driving forces, *Nature, 378,* 25-31, 1995.

van der Hilst, R.D., S. Widiyantoro, and E.R. Engdahl, Evidence for deep mantle circulation from global tomography, *Nature, 386,* 578-584, 1997.

van Keken, P.E., and C.J. Ballentine, Dynamical models of mantle volatile evolution and the role of phase transitions and temperature-dependent rheology, *J. Geophys. Res., 104,* 7137-7168, 1999.

van Keken, P.E., and S. Zhong, Mixing in a 3D spherical model of present-day mantle convection, *Earth Planet. Sci. Lett., 171,* 533-547, 1999.

van Keken, P.E., S. Karato, and D.A. Yuen, Rheological control of oceanic crust separation in the transition zone, *Geophys. Res. Lett., 23,* 1821-1824, 1996.

White, R.S., and D. McKenzie, Mantle plumes and flood basalts, *J. Geophys. Res., 100,* 17,543-17,585, 1995.

Yasuda, A., T. Fujii, and K. Kurita, Melting phase relations of an anhydrous mid-ocean ridge basalt from 3 to 20 GPa: Implications for the behavior of subducted oceanic crust in the mantle, *J. Geophys. Res., 99,* 9401-9414, 1994.

Yaxley, G.M., and D.H. Green, Reactions between eclogite and peridotite: Mantle refertilisation by subduction of oceanic crust, *Schweiz. Mineral. Petrogr. Mitt., 78,* 243-255, 1998.

G. F. Davies, Research School of Earth Sciences, Australian National University, Canberra, ACT 0200, Australia. (Geoff.Davies@anu.edu.au)

A. M. Leitch, Department of Earth Sciences, Memorial University of Newfoundland, St. John's, A1B 3X5, Newfoundland, Canada. (aleitch@waves.esd.mun.ca)

(Received September 7, 1999; revised June 7, 2000;
accepted August 17, 2000.)